

Constraints on the Local Cosmic Void from the Pantheon Supernovae Data

Ke Wang^{1,2,3*} and Kun-Peng Chen^{1†}

¹*School of Physical Science and Technology, Lanzhou University, Lanzhou 730000, China*

²*Lanzhou Center for Theoretical Physics, Key Laboratory of Theoretical Physics of Gansu Province, Lanzhou University, Lanzhou 730000, China and*

³*Institute of Theoretical Physics & Research Center of Gravitation, Lanzhou University, Lanzhou 730000, China*

(Dated: April 28, 2023)

In principle, the local cosmic void can be simply modeled by the spherically symmetric Lemaitre-Tolman-Bondi (LTB) metric. In practice, the real local cosmic void is probably not spherically symmetric. In this paper, to reconstruct the realistic profile of the local cosmic void, we divide it into several segments. Each segment with certain solid angle is modeled by its own LTB metric. Meanwhile, we divide the 1048 type Ia supernovae (SNIa) of Pantheon into corresponding subsets according to their distribution in the galactic coordinate system. Obviously, each SNIa subset can only be used to reconstruct the profile of one segment. Finally, we can patch together an irregular profile for the local cosmic void with the whole Pantheon sample. But our constraints are too weak to challenge the cosmic homogeneity and the cosmic isotropy.

I. INTRODUCTION

The cosmological principle assumes that the universe is homogeneous and isotropic on cosmic scales. Based on this assumption as well as the standard model of particle physics and Einstein's general relativity (GR), the Lambda cold dark matter (Λ CDM) model is proposed. This standard model of cosmology has proved successful on large cosmic scales according to the latest cosmic microwave background (CMB) observations, namely Planck 2018 data [1]. However, it faces major challenges on small scales, such as the Hubble tension [2] and the dipolar tension [3]. Besides GR, dark energy model or treatments of systematic uncertainty, the former tension also challenges the local cosmic homogeneity and the latter one also challenges the cosmic isotropy on small scales. Therefore, a further test of the local cosmic inhomogeneity and the cosmic anisotropy on small scales is necessary.

The local cosmic inhomogeneity can be simply modeled by the spherically symmetric Lemaitre-Tolman-Bondi (LTB) metric [4–6]. Taking the late-time matter and dark energy into consideration, there is an Λ CDM model's counterpart, namely Λ LTB model. Using the combination of the latest available cosmological observations, the local radial inhomogeneity in the Λ LTB model has been probed [7, 8]. Even though a deeper local void can reconcile the Hubble tension [9] and a larger local void can reconcile the dipolar tension [10], a shallower and smaller local void is favored by the combination of the latest available cosmological observations [7, 8]. Moreover, a spherically symmetric local cosmic inhomogeneity may not meet the reality. Therefore, in this paper, we will probe the true profile of the local cosmic inhomogeneity as realistic as possible.

The cosmic anisotropy on small scales can be tested by

type Ia supernovae (SNIa) data, such as the combined Pantheon sample [11]. One straightforward method is to divide the whole samples into several subsets according to the distribution of individual SNIa in the galactic coordinate system. In particular hemisphere comparison method [12, 13] divides the whole sample into two data subsets which are from “up” hemisphere and “down” hemisphere respectively [14–16]. Also, HEALPix [17] can be used to divide the whole sample into more data subsets [16, 18, 19]. Another common method is the dipole fitting method [20], which assumes a priori dipole in the cosmic anisotropy on small scales [14–16, 21, 22]. Until now, there is no evidence for the cosmic anisotropy on small scales in the SNIa samples. However, these null signals are just overall constraints and may neglect some fine structures in the universe.

In this paper, we try to test both of the local cosmic inhomogeneity and the cosmic anisotropy on small scales at the same time using the SNIa data of Pantheon. To account for the asymmetry in the local cosmic inhomogeneity and the fine structures in the cosmic anisotropy on small scales, we will search for the cosmic anisotropy on small scales with the Λ LTB model. First, we cut the local cosmic void into several segments. Each segment with certain solid angle is modeled by its own LTB metric. Then, we divide the 1048 SNIa of Pantheon into corresponding subsets according to their distribution in the galactic coordinate system. Obviously, each SNIa subset can only be used to reconstruct the profile of one segment. Finally, we can patch together an irregular profile for the local cosmic void with the whole Pantheon sample. The whole profile will contain all the information about both of the local cosmic inhomogeneity and the cosmic anisotropy on small scales.

This paper is organized as follows. In section II, we present our method of modeling the local cosmic inhomogeneity and introduce our treatment of the Pantheon data. In section III, we show the constraints on the profiles of all segments of the local cosmic inhomogeneity and compare them. Finally, a brief summary and discussions

*Corresponding author: wangkey@lzu.edu.cn

†chenkp19@lzu.edu.cn

are included in section IV.

II. METHODOLOGY AND DATA

A. Model

A spherically symmetric void can be simply modeled by the LTB metric

$$ds^2 = -dt^2 + \frac{R'^2(r, t)}{1 + 2r^2 k(r) \tilde{M}^2} dr^2 + R^2(r, t) d\Omega, \quad (1)$$

where $d\Omega = d\theta^2 + \sin^2 \theta d\phi^2$, \tilde{M} is an arbitrary mass scale, $k(r)$ is an arbitrary curvature profile function, $R(r, t) = a(t)r$ is dependent on the FLRW scale factor $a(t)$ and a prime (or dot) denotes derivative with respect to the radial coordinate r (or the time t). As Λ CDM model is built on the FLRW metric, there is a Λ LTB model built on the LTB metric. The universe's expansion in the Λ LTB model is determined by a Friedmann-like equation

$$\frac{\dot{R}^2(r, t)}{R^2(r, t)} = \frac{2m(r)}{R^3(r, t)} + \frac{2r^2 k(r) \tilde{M}^2}{R^2(r, t)} + \frac{\Lambda}{3}, \quad (2)$$

where $m(r)$ is the so-called Euclidean mass function and be set as $m(r) = 4\pi \tilde{M}^2 r^3 / 3$, the Big Bang time $t_{\text{BB}}(r)$ is fixed as a constant and the curvature profile $k(r)$ is the only free function to determine the void. More precisely, there is a transverse expansion rate and a longitudinal expansion rate. The former one is dependent on a transverse scale factor $a_{\perp}(r, t) = R(r, t)/r$ as

$$H_{\perp}(r, t) = \frac{\dot{a}_{\perp}(r, t)}{a_{\perp}(r, t)}, \quad (3)$$

the latter one is dependent on a longitudinal scale factor $a_{\parallel}(r, t) = R'(r, t)$ as

$$H_{\parallel}(r, t) = \frac{\dot{a}_{\parallel}(r, t)}{a_{\parallel}(r, t)}. \quad (4)$$

According to the above Friedmann-like equation, we can define the density parameters of matter, curvature and dark energy today as

$$\Omega_m(r) = \frac{2m(r)}{R^3(r, t_0) H_{\perp}^2(r, t_0)}, \quad (5)$$

$$\Omega_k(r) = \frac{2r^2 k(r) \tilde{M}^2}{R^2(r, t_0) H_{\perp}^2(r, t_0)}, \quad (6)$$

$$\Omega_{\Lambda}(r) = \frac{\Lambda}{3H_{\perp}^2(r, t_0)}. \quad (7)$$

The profile of the void can be parameterized by the depth and size of the void and the width of the void boundary [23]. In fact, the depth and size of the void

are enough and the width of the void boundary can be ignored [24]

$$k(r) = k_c P_3(r), \quad (8)$$

$$P_n(r) = \begin{cases} 1 - \exp\left[\frac{-(1-r/r_B)^n}{r/r_B}\right] & 0 \leq r < r_B \\ 0 & r_B \leq r \end{cases}, \quad (9)$$

where we have assumed the universe is flat outside the void, k_c is the curvature at the center and r_B is the comoving radius of the void.

If the void is spherically symmetric and the all latest available cosmological observations are on hand, the profile at r can be constrained by data from any direction or sky location. Therefore, the depth of the void and the boundary of the void in particular where the curvature changes to 0 can be constrained relatively well [7]. If only SNIa data is used to probe the asymmetry of the void, however, we find the depth of the void still can be constrained relatively well but the boundary of the void where the curvature changes to 0 can't be constrained. Therefore, we introduce a r_C where the curvature changes by 10%. That is to say, we will not attempt to obtain the information about the whole void but conservatively concentrate on the partial profile of the void by the following function:

$$P_n(r) = \begin{cases} 1 - 0.1 \exp\left[\frac{-(1-r/r_C)^n}{r/r_C}\right] & 0 \leq r < r_C \\ 0.9 \left[1 - \exp\left[\frac{-\left(1 - \frac{r-r_C}{r_B-r_C}\right)^n}{\frac{r-r_C}{r_B-r_C}}\right] \right] & r_C \leq r < r_B \\ 0 & r_B \leq r \end{cases}. \quad (10)$$

Now, the void is parameterized by three parameters $\{k_c, r_C, r_B\}$. All of them are derived parameters in our code. k_c is related to $\tilde{\delta}_0 = \tilde{\delta}(r=0, t_0)$, where the integrated mass density contrast $\tilde{\delta}(r, t_0)$ [7] is defined as

$$\tilde{\delta}(r, t_0) = \frac{\Omega_m H_{\perp}^2}{\Omega_m^{\text{out}} H_0^{\text{out}2}} - 1, \quad (11)$$

where ‘‘out’’ denotes the corresponding FLRW quantities. Because $-1 \leq \tilde{\delta}_0 < \infty$ is not good for the convergence of the Monte Carlo Markov Chain (MCMC), we will use a new parameter

$$\delta_0 = \begin{cases} \tilde{\delta}_0 & \tilde{\delta}_0 \leq 0 \\ \tilde{\delta}_0 / (1 + \tilde{\delta}_0) & \tilde{\delta}_0 > 0 \end{cases}. \quad (12)$$

As for the other two radii $\{r_B, r_C\}$, we will relate them to their corresponding redshifts by $r_B = r(z_B)$ and $r_C = r(z_C)$, where $r(z)$ satisfies the geodesic equations

$$\frac{dt}{dz} = -\frac{R'(r, t)}{(1+z)\dot{R}'(r, t)}, \quad (13)$$

$$\frac{dr}{dz} = -\frac{\sqrt{1 + 2r^2 k(r) \tilde{M}^2}}{(1+z)\dot{R}'(r, t)}. \quad (14)$$

As mentioned before, the information about the whole void is out of reach of SNIa data. Therefore, we further relate r_B to r_C as $r_B = 2r_C$. That is to say, we will only conservatively concentrate on the profile of the void when $z \leq z_C$ and the profile of the void when $z_C < z \leq z_B$ is set by our assumption $r_B = 2r_C$. Moreover, $z_B > 0$ is meaningless when $\delta_0 \sim 0$. So, we relate z_B to $|\delta_0|$ by a free parameter $|z_B/\delta_0|$ which will have a uniform prior distribution $|z_B/\delta_0| \in [0, 100]$. The other free parameter δ_0 will have a uniform prior distribution $\delta_0 \in [-0.99, 0.99]$. Finally, we can use the dependence of SNIa's luminosity distance on these two void parameters $\{\delta_0, z_B = |\delta_0| \times |z_B/\delta_0|\}$ to probe the profile of the void, where the angular diameter distance d_A and the luminosity distance d_L are obtained

$$d_A(z; \delta_0, z_B) = R(r(z), t(z); \delta_0, z_B), \quad (15)$$

$$d_L(z; \delta_0, z_B) = (1 + z)^2 d_A(z; \delta_0, z_B). \quad (16)$$

B. Data

In this paper, we only use the combined Pantheon sample [11] to constrain the local cosmic void. This dataset consists of 1048 SNIa in the redshift range $0.01 < z < 2.3$. In Fig. 1, we show the distribution of these 1048 SNIa in the galactic coordinate system (l, b) . To probe the asymmetry in the local cosmic inhomogeneity, we divide the full dataset into several subsets further, as listed in Tab. I. Obviously, each SNIa subset can only give the local information of the universe which can be characterized by a corresponding LTB metric. This is to say, the whole profile of the local cosmic void should be reconstructed with the full SNIa dataset and described by several corresponding LTB metrics. Therefore, for no cut case, we have

$$\chi^2 = \chi_{\text{P}_{\text{All}}}^2; \quad (17)$$

for one horizontal cut case, we have

$$\chi^2 = \chi_{\text{P}_{\text{N}}}^2 + \chi_{\text{P}_{\text{S}}}^2; \quad (18)$$

for one vertical cut case, we have

$$\chi^2 = \chi_{\text{P}_{\text{E}}}^2 + \chi_{\text{P}_{\text{W}}}^2; \quad (19)$$

for two cuts case, we have

$$\chi^2 = \chi_{\text{P}_{\text{NE}}}^2 + \chi_{\text{P}_{\text{NW}}}^2 + \chi_{\text{P}_{\text{SE}}}^2 + \chi_{\text{P}_{\text{SW}}}^2. \quad (20)$$

The χ_s^2 for every data subset is

$$\chi_s^2 = \sum (\mathbf{m}_{\text{B},s}^{\text{obs}} - \mathbf{m}_{\text{B},s}^{\text{mod}})^T (\mathbf{C})_s^{-1} (\mathbf{m}_{\text{B},s}^{\text{obs}} - \mathbf{m}_{\text{B},s}^{\text{mod}}), \quad (21)$$

where \mathbf{C}_s is the covariance matrix of the s -th subset, the apparent magnitude $\mathbf{m}_{\text{B},s}^{\text{obs}}$ observed by Pantheon has included the contribution of stretch x_1 , color c and

TABLE I: According to the distribution of 1048 SNIa of Pantheon [11] in the galactic coordinate system (l, b) , the full dataset is divided into $\text{P}_{\text{N}}+\text{P}_{\text{S}}$ by one horizontal cut, $\text{P}_{\text{E}}+\text{P}_{\text{W}}$ by one vertical cut and $\text{P}_{\text{NE}}+\text{P}_{\text{NW}}+\text{P}_{\text{SE}}+\text{P}_{\text{SW}}$ by two cuts separately.

Dataset	l	b
P_{All}	$0^\circ \leq l < 360^\circ$	$-90^\circ \leq b \leq 90^\circ$
P_{N}	$0^\circ \leq l < 360^\circ$	$0^\circ \leq b \leq 90^\circ$
P_{S}	$0^\circ \leq l < 360^\circ$	$-90^\circ \leq b < 0^\circ$
P_{W}	$0^\circ \leq l \leq 180^\circ$	$-90^\circ \leq b \leq 90^\circ$
P_{E}	$180^\circ < l < 360^\circ$	$-90^\circ \leq b \leq 90^\circ$
P_{NW}	$0^\circ \leq l \leq 180^\circ$	$0^\circ \leq b \leq 90^\circ$
P_{NE}	$180^\circ < l < 360^\circ$	$0^\circ \leq b \leq 90^\circ$
P_{SW}	$0^\circ \leq l \leq 180^\circ$	$-90^\circ \leq b < 0^\circ$
P_{SE}	$180^\circ < l < 360^\circ$	$-90^\circ \leq b < 0^\circ$

TABLE II: The Λ CDM model's six parameters given by Planck 2018 TT,TE,EE+lowE+lensing [1].

$\Omega_b h^2$	$\Omega_c h^2$	$H_0 [\text{km s}^{-1} \text{Mpc}^{-1}]$	τ	$\ln 10^{10} A_s$	n_s
0.02237	0.12	67.36	0.0544	3.044	0.9649

host-galaxy correction ΔM and the apparent magnitude $m_{\text{B},s,i}^{\text{mod}}$ for the i -th SNIa of the s -th subset in the Λ LTB model is dependent on two void parameters $\{\delta_{0,s}, z_{\text{B},s}\}$ and the absolute magnitude M_{B} as

$$m_{\text{B},s,i}^{\text{mod}}(z_i; \delta_{0,s}, z_{\text{B},s}, M_{\text{B}}) = 5 \log_{10} \frac{d_L(z_i; \delta_{0,s}, z_{\text{B},s})}{1 \text{Mpc}} + 25 + M_{\text{B}}. \quad (22)$$

Since SNIa are supposed to be standard candles, we should exclude the effects of variations of M_{B} in each SNIa subset on the asymmetry in the local cosmic inhomogeneity. Therefore, for every cut case, we use the full dataset to constrain the only nuisance parameter M_{B} .

III. RESULTS

The luminosity distance $d_L(z; \delta_0, z_{\text{B}})$ in the Λ LTB model is numerically given by VoidDistances2020 [26] which should be fed with parameters about the universe outside the void. The initialization of the universe outside the void is done by CLASS [27], even though we don't use the CMB data here. For CLASS [27], we need to provide the Λ CDM model's six parameters. In Tab. II, we list the Λ CDM model's six parameters given by Planck 2018 TT,TE,EE+lowE+lensing [1]. Finally, the likelihoods in subsection II B are added into MontePython [25] by our modified monteLLTB [7].

In Tab. III, the constraints on $\{\delta_{0,s}, z_{\text{C},s}, M_{\text{B}}\}$ with every data subset are summarized. In Fig. 2, Fig. 3, Fig. 4 and Fig. 5, the constraints on $\{\delta_{0,s}, z_{\text{C},s}, M_{\text{B}}\}$ with every data subset for no cut case, one horizontal cut case, one vertical cut case and two cuts case are also shown

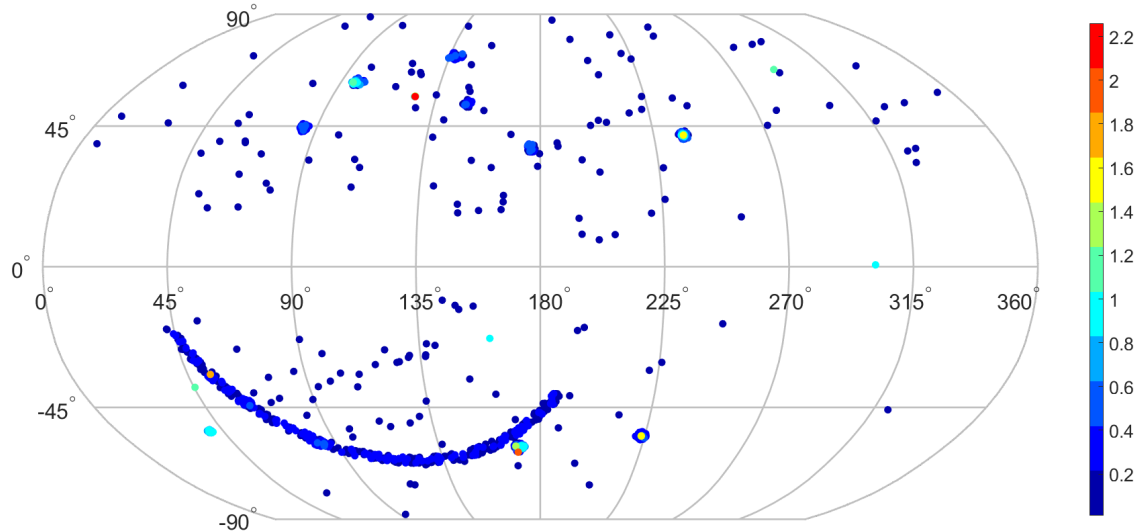


FIG. 1: The distribution of 1048 SNIa of Pantheon in the galactic coordinate system (l, b), where the discrete colorbar indicates the redshifts of these SNIa.

respectively. Since the only nuisance parameter M_B is constrained with the full dataset for all cut cases, M_B almost shares the same constraint for every cut case. Although we suppose $\delta_{0,s}$ of every LTB metric is only constrained with the corresponding data subset and there is no correlation between $\delta_{0,s}$, for any cut case, there is an obvious correlation between $\delta_{0,s}$ in Fig. 3, Fig. 4 and Fig. 5. That is because we have supposed SNIa are standard candles and all $\delta_{0,s}$ directly correlates with M_B and indirectly correlates with the other $\delta_{0,s}$. For every cut case, the correlation between $\delta_{0,s}$ just leads to a similar error of $\delta_{0,s}$ $0.08 \sim 0.10$ but imposes no effect on the mean value of $\delta_{0,s}$. Generally speaking, for all cut cases, the constraints on $\delta_{0,s}$ are consistent with the FLRW metric at 95% confidence level (CL): on the one hand, the constraints on $\delta_{0,s}$ are consistent with 0, which means the cosmic homogeneity; on the other hand, the constraints on $\delta_{0,s}$ are consistent with each other, which means the cosmic isotropy. However, the constraint on $\delta_{0,PSE} = -0.15 \pm 0.08$ deviates from 0 at almost 2σ . This deviation results from either the paucity of data in P_{SE} data subset or the real depth of the local cosmic void in this direction. Even though we have given up the profile at $z_C \leq z < z_B$ by setting $r_B = 2r_C$, the constraints on $z_{C,s}$ are still very weak. Except for a peak at $z_{C,s} = 0$, there is another peak at $1 \lesssim z_{C,s} \lesssim 2.26$. But we can't conclude that the Pantheon data prefers a non-zero $z_{C,s}$ to $z_{C,s} = 0$.

Finally, we can use the constraints on $\{\delta_{0,s}, z_{C,s}\}$ for every cut case to probe both of the local cosmic inho-

TABLE III: The constraints on void parameters and the absolute magnitude.

Dataset	δ_0 (68%)	z_C (95%)	M_B (68%)
P_{All}	-0.05 ± 0.10	< 1.97	-19.41 ± 0.04
P_N	-0.11 ± 0.09	< 2.16	-19.40 ± 0.03
P_S	-0.07 ± 0.09	< 2.05	-19.40 ± 0.03
P_W	-0.08 ± 0.09	< 2.02	-19.40 ± 0.03
P_E	-0.11 ± 0.09	< 2.28	-19.40 ± 0.03
P_{NW}	-0.11 ± 0.08	< 2.16	-19.40 ± 0.03
P_{NE}	-0.09 ± 0.09	< 2.10	-19.40 ± 0.03
P_{SW}	-0.06 ± 0.08	< 1.88	-19.40 ± 0.03
P_{SE}	-0.15 ± 0.08	< 2.34	-19.40 ± 0.03

mogeneity and the cosmic anisotropy on small scales. In Fig. 6, Fig. 7 and Fig. 8, we reconstruct the profile of local cosmic void $\delta(z, t_0)$ in different direction (solid lines) with the constraints summarized in Tab. III. At $z \lesssim z_{C,s}$ (dashed lines), the curvature changes by 10%. And we complete the rest of profile until $z_{B,s}$ (dotted lines) by setting $r_B = 2r_C$. We find that even a small difference between $z_{C,s}$ can lead to a large difference between $z_{B,s}$ when the void is deeper at the center. And a deeper void (or a smaller $\delta_{0,s}$) usually prefers a wider void (or a larger $z_{B,s}$). Therefore, even a smaller local cosmic inhomogeneity at the center of a deeper void can lead to a larger cosmic anisotropy at the boundary of this void.

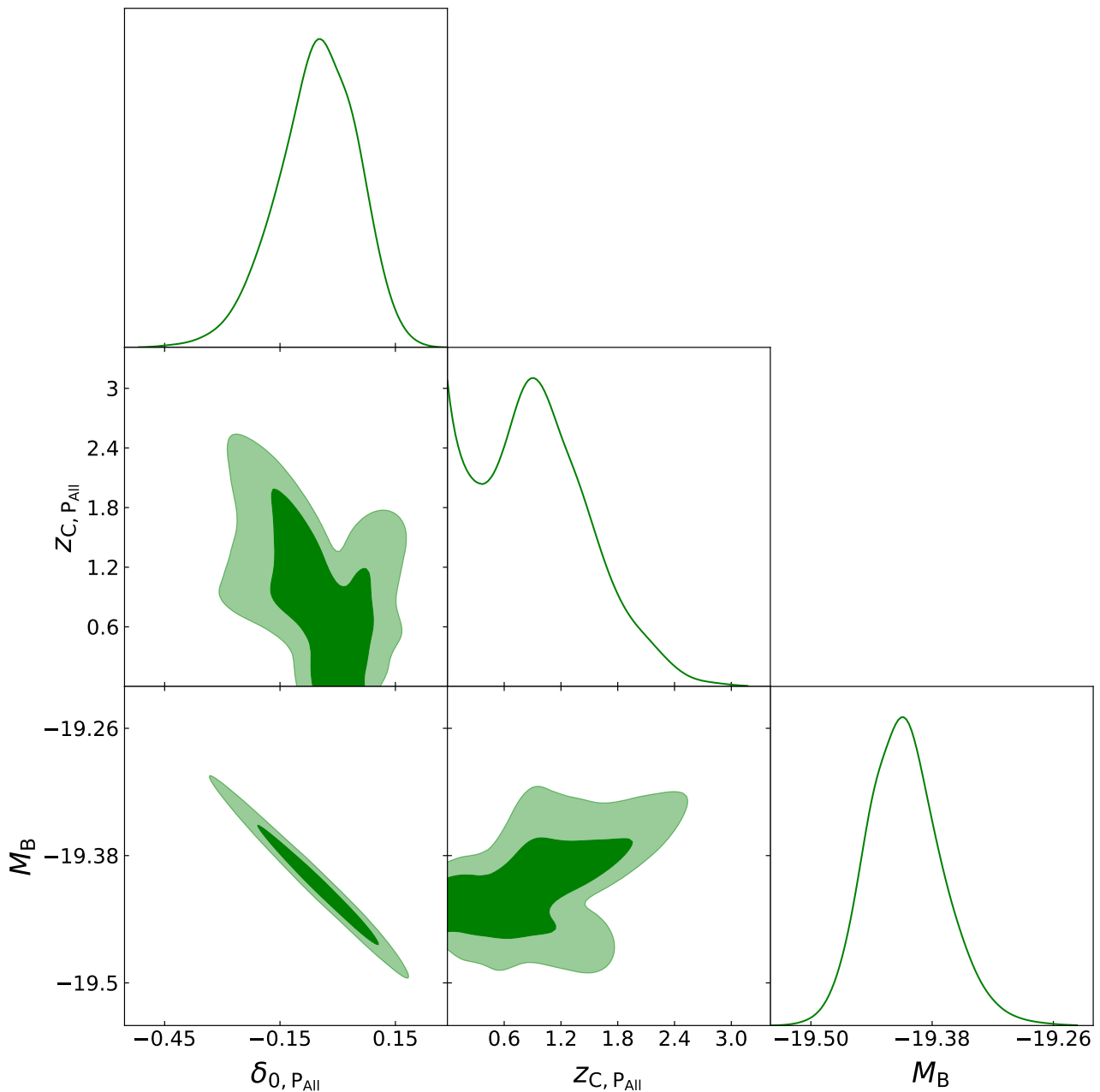


FIG. 2: The triangular plot of void parameters and M_B for no cut case, where the contours show 68% and 95% confidence ranges.

IV. SUMMARY AND DISCUSSION

In this paper, we try to test both of the local cosmic inhomogeneity and the cosmic anisotropy on small scales at the same time using the SNIa data of Pantheon. Similar to the hemisphere comparison method, but with the LTB metric instead of the FLRW metric, we first divide the full dataset into several date subsets and then use the date subsets to constrain the void parameters $\{\delta_{0,s}, z_{C,s}\}$ in the corresponding direction. Due to the

paucity of data, we just concentrate on the profile of the void at $z < z_C$ where the curvature changes by 10%. Even though we turn to this trick, we just can constrain $\delta_{0,s}$ well but can't constrain $z_{C,s}$ well. The constraints on $\delta_{0,s}$ for all cut cases are consistent with the FLRW metric at 95% CL. The constraints on $z_{C,s}$ for all cut cases are almost beyond 2.26 at 95% CL. That is to say, our constraints are too weak to challenge the cosmic homogeneity and the cosmic isotropy. If the local cosmic void dose exist, however, even a smaller cosmic inhomogeneity

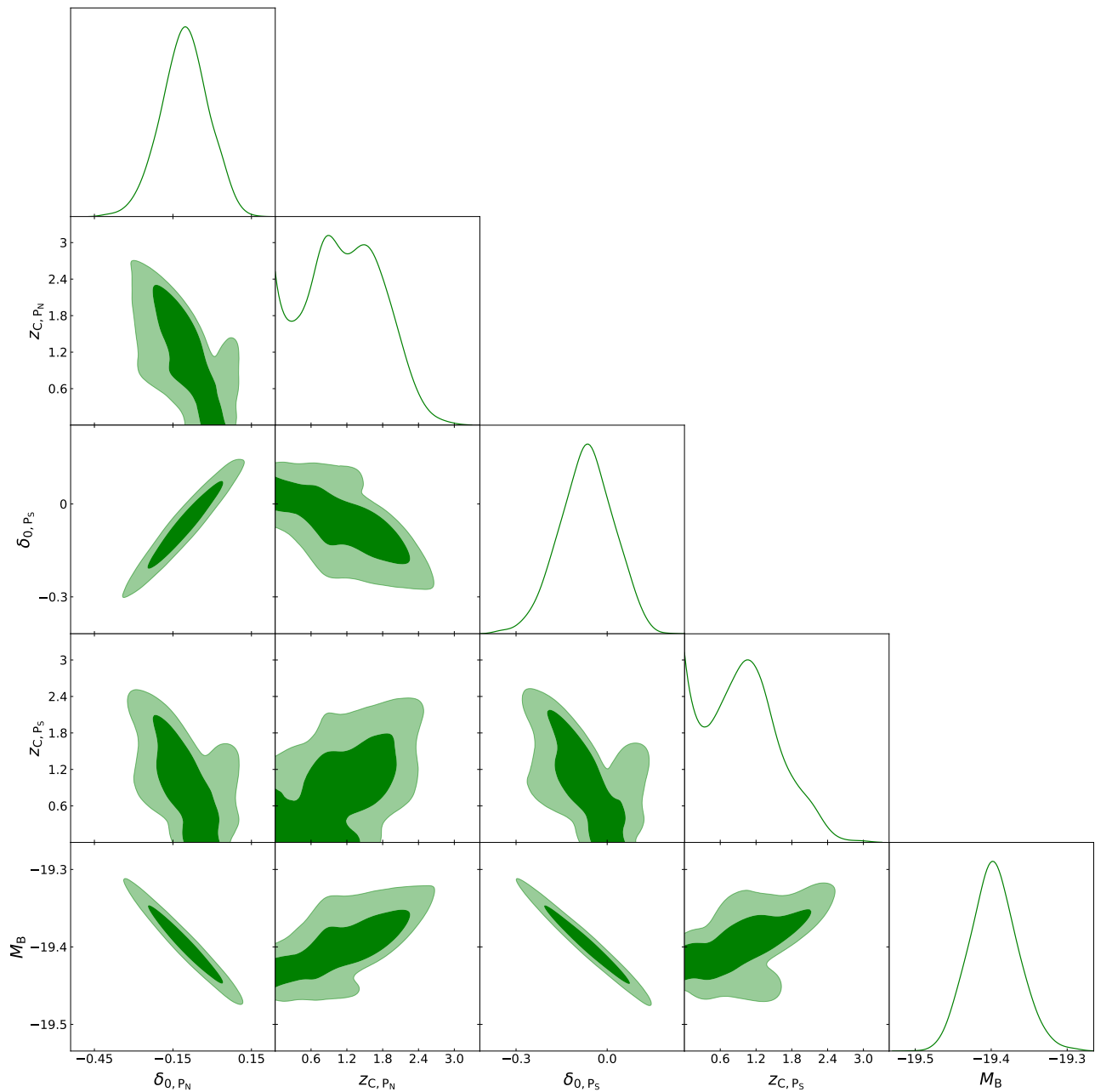


FIG. 3: The triangular plot of void parameters and M_B for one horizontal cut case, where the contours show 68% and 95% confidence ranges.

at the center of a deeper void can lead to a larger cosmic anisotropy at the boundary of this void.

Although our results are consistent with the cosmic homogeneity and the cosmic isotropy at 95% CL, there are some deviations from FLRW metric at 68% CL. These deviations result from either the paucity of data in the data subset or the real physics in the corresponding direction. Therefore, more SNIa observations or other cosmological observations are needed to alleviate the paucity of data in certain directions.

Acknowledgments

We acknowledge the use of HPC Cluster of Tianhe II in National Supercomputing Center in Guangzhou. Ke Wang is supported by grants from NSFC (grant No. 12005084 and grant No.12247101) and grants from the China Manned Space Project with NO. CMS-CSST-2021-B01.

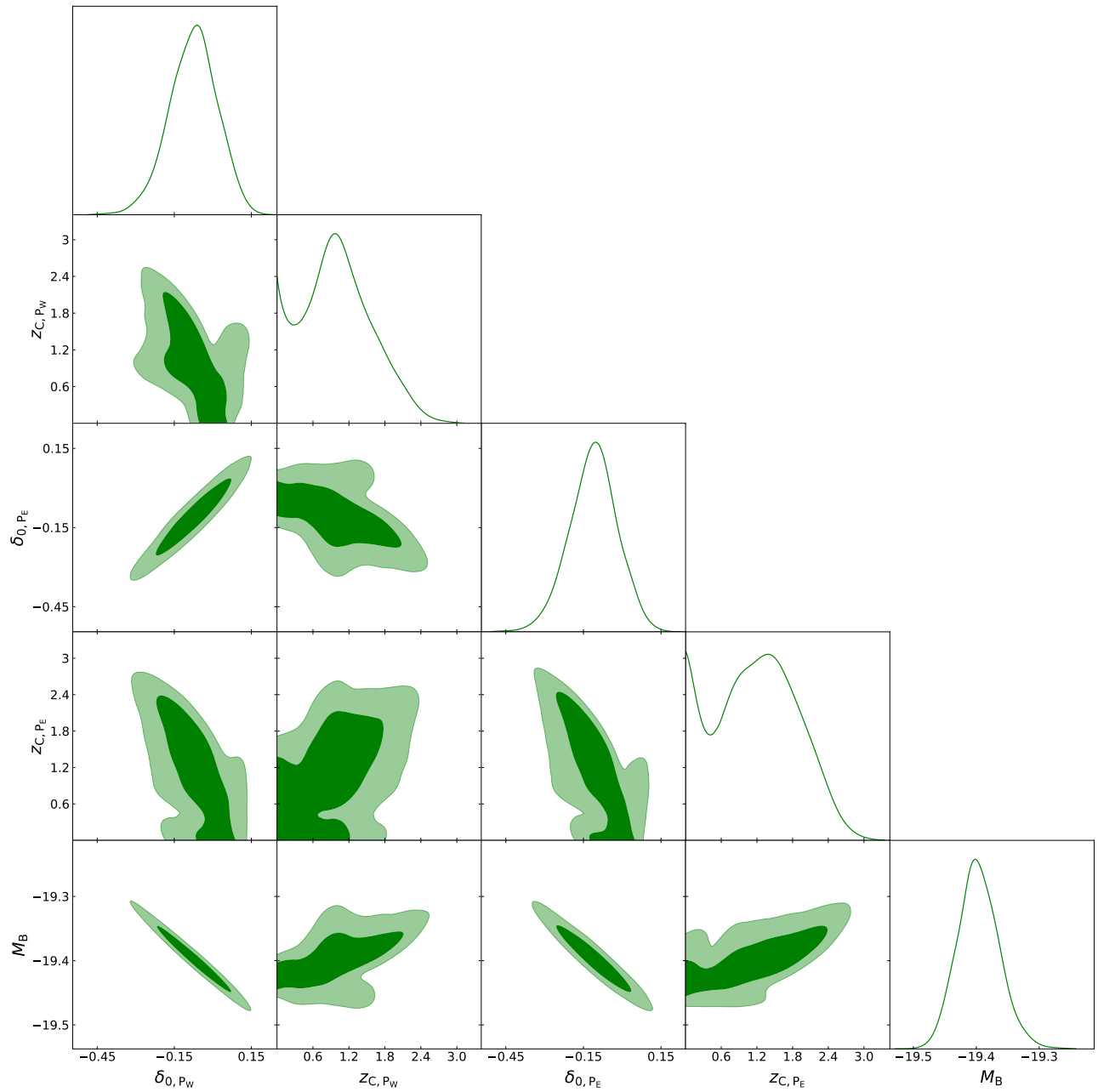


FIG. 4: The triangular plot of void parameters and M_B for one vertical cut case, where the contours show 68% and 95% confidence ranges.

-
- [1] N. Aghanim *et al.* [Planck], “Planck 2018 results. VI. Cosmological parameters,” *Astron. Astrophys.* **641**, A6 (2020) [erratum: *Astron. Astrophys.* **652**, C4 (2021)] [arXiv:1807.06209 [astro-ph.CO]].
- [2] A. G. Riess, S. Casertano, W. Yuan, L. M. Macri and D. Scolnic, “Large Magellanic Cloud Cepheid Standards Provide a 1% Foundation for the Determination of the Hubble Constant and Stronger Evidence for Physics beyond Λ CDM,” *Astrophys. J.* **876**, no.1, 85 (2019) [arXiv:1903.07603 [astro-ph.CO]].
- [3] N. J. Secrest, S. von Hausegger, M. Rameez, R. Mohayaee, S. Sarkar and J. Colin, “A Test of the Cosmological Principle with Quasars,” *Astrophys. J. Lett.* **908**, no.2, L51 (2021) [arXiv:2009.14826 [astro-ph.CO]].
- [4] G. Lemaitre, “The expanding universe,” *Annales Soc. Sci. Bruxelles A* **53**, 51-85 (1933)

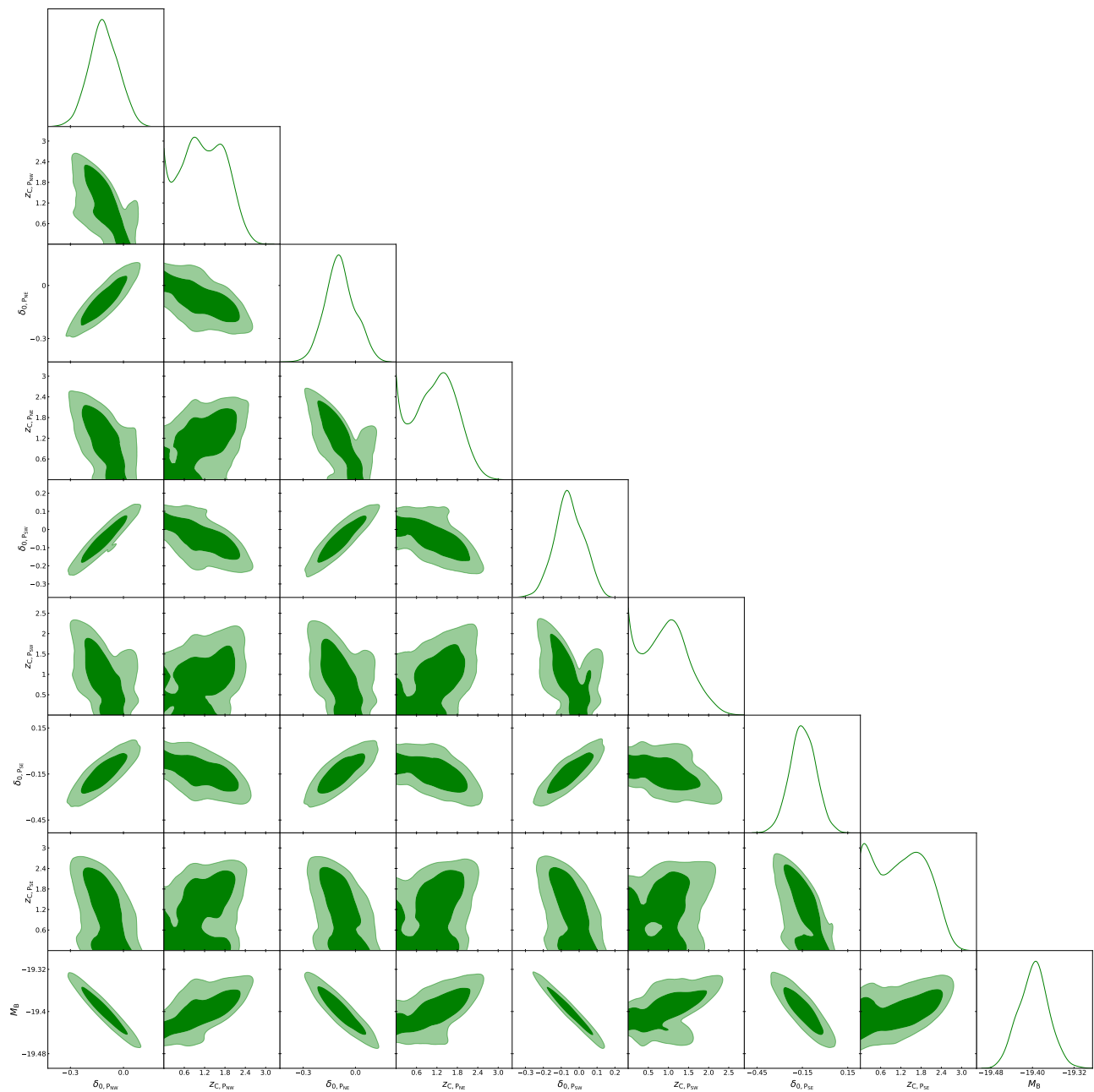


FIG. 5: The triangular plot of void parameters and M_B for two cuts case, where the contours show 68% and 95% confidence ranges.

- [5] R. C. Tolman, “Effect of inhomogeneity on cosmological models,” *Proc. Nat. Acad. Sci.* **20**, 169-176 (1934)
- [6] H. Bondi, “Spherically symmetrical models in general relativity,” *Mon. Not. Roy. Astron. Soc.* **107**, 410-425 (1947)
- [7] D. Camarena, V. Marra, Z. Sakr and C. Clarkson, “The Copernican principle in light of the latest cosmological data,” *Mon. Not. Roy. Astron. Soc.* **509**, no.1, 1291-1302 (2021) [arXiv:2107.02296 [astro-ph.CO]].
- [8] D. Camarena, V. Marra, Z. Sakr and C. Clarkson, “A void in the Hubble tension? The end of the line for the Hubble bubble,” *Class. Quant. Grav.* **39**, no.18, 184001 (2022) [arXiv:2205.05422 [astro-ph.CO]].
- [9] V. Marra, L. Amendola, I. Sawicki and W. Valkenburg, “Cosmic variance and the measurement of the local Hubble parameter,” *Phys. Rev. Lett.* **110**, no.24, 241305 (2013) [arXiv:1303.3121 [astro-ph.CO]].
- [10] T. Cai, Q. Ding and Y. Wang, “Reconciling cosmic dipolar tensions with a gigaparsec void,” [arXiv:2211.06857 [astro-ph.CO]].
- [11] D. M. Scolnic *et al.* [Pan-STARRS1], “The Complete Light-curve Sample of Spectroscopically Confirmed SNe

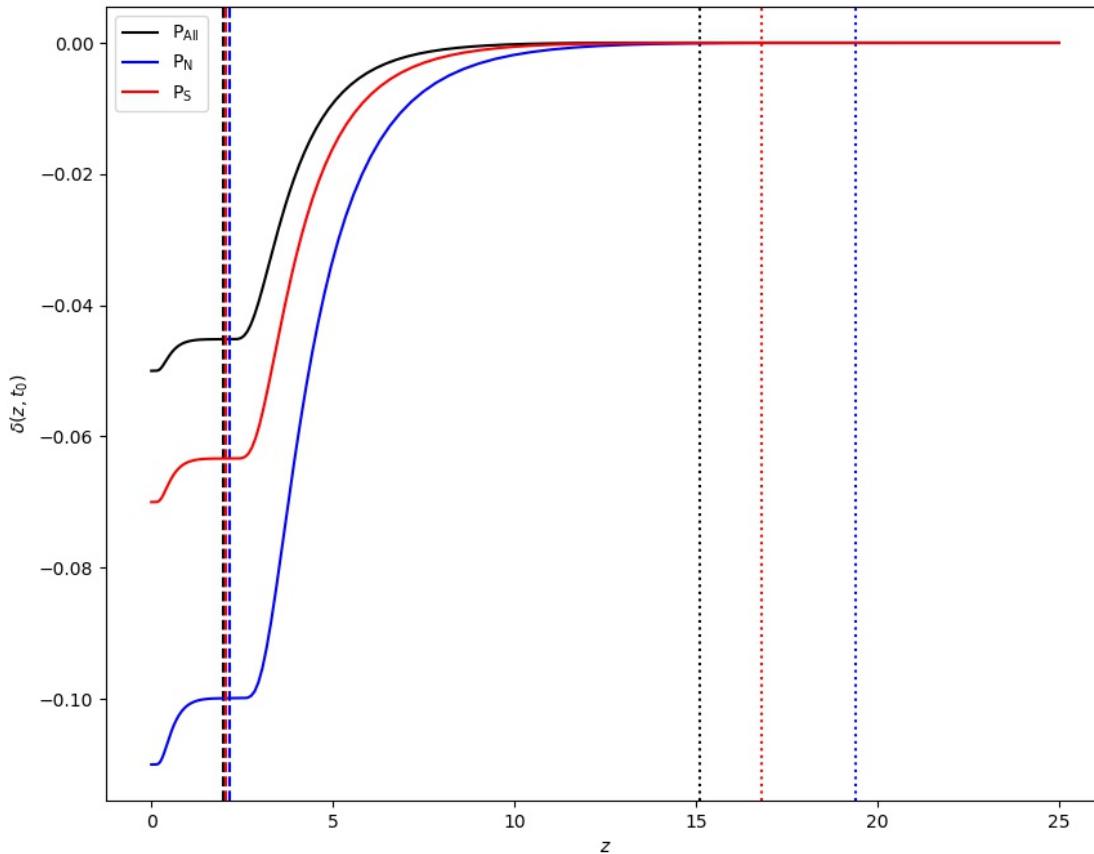


FIG. 6: The integrated mass density contrast $\delta(z, t_0)$ for no cut case and one horizontal cut case, where $\delta_0 = -0.05$ (black solid), $z_C = 1.97$ (black dashed) and $z_B = 15.1$ (black dotted) for P_{All} , $\delta_0 = -0.11$ (blue solid), $z_C = 2.16$ (blue dashed) and $z_B = 19.4$ (blue dotted) for P_N and $\delta_0 = -0.07$ (red solid), $z_C = 2.05$ (red dashed) and $z_B = 16.8$ (red dotted) for P_S respectively.

- Ia from Pan-STARRS1 and Cosmological Constraints from the Combined Pantheon Sample,” *Astrophys. J.* **859**, no.2, 101 (2018) [arXiv:1710.00845 [astro-ph.CO]].
- [12] D. J. Schwarz and B. Weinhorst, “(An)isotropy of the Hubble diagram: Comparing hemispheres,” *Astron. Astrophys.* **474**, 717-729 (2007) [arXiv:0706.0165 [astro-ph]].
- [13] I. Antoniou and L. Perivolaropoulos, “Searching for a Cosmological Preferred Axis: Union2 Data Analysis and Comparison with Other Probes,” *JCAP* **12**, 012 (2010) [arXiv:1007.4347 [astro-ph.CO]].
- [14] H. K. Deng and H. Wei, “Testing the Cosmic Anisotropy with Supernovae Data: Hemisphere Comparison and Dipole Fitting,” *Phys. Rev. D* **97**, no.12, 123515 (2018) [arXiv:1804.03087 [astro-ph.CO]].
- [15] Z. Q. Sun and F. Y. Wang, “Testing the anisotropy of cosmic acceleration from Pantheon supernovae sample,” *Mon. Not. Roy. Astron. Soc.* **478**, no.4, 5153-5158 (2018) [arXiv:1805.09195 [astro-ph.CO]].
- [16] H. K. Deng and H. Wei, “Null signal for the cosmic anisotropy in the Pantheon supernovae data,” *Eur. Phys. J. C* **78**, no.9, 755 (2018) [arXiv:1806.02773 [astro-ph.CO]].
- [17] K. M. Górski, E. Hivon, A. J. Banday, B. D. Wandelt, F. K. Hansen, M. Reinecke and M. Bartelman, “HEALPix - A Framework for high resolution discretization, and fast analysis of data distributed on the sphere,” *Astrophys. J.* **622**, 759-771 (2005) [arXiv:astro-ph/0409513 [astro-ph]].
- [18] U. Andrade, C. A. P. Bengaly, B. Santos and J. S. Alcaniz, “A Model-independent Test of Cosmic Isotropy with Low-z Pantheon Supernovae,” *Astrophys. J.* **865**, no.2, 119 (2018) [arXiv:1806.06990 [astro-ph.CO]].
- [19] W. Zhao, P. X. Wu and Y. Zhang, “Anisotropy of Cosmic Acceleration,” *Int. J. Mod. Phys. D* **22**, 1350060 (2013) [arXiv:1305.2701 [astro-ph.CO]].

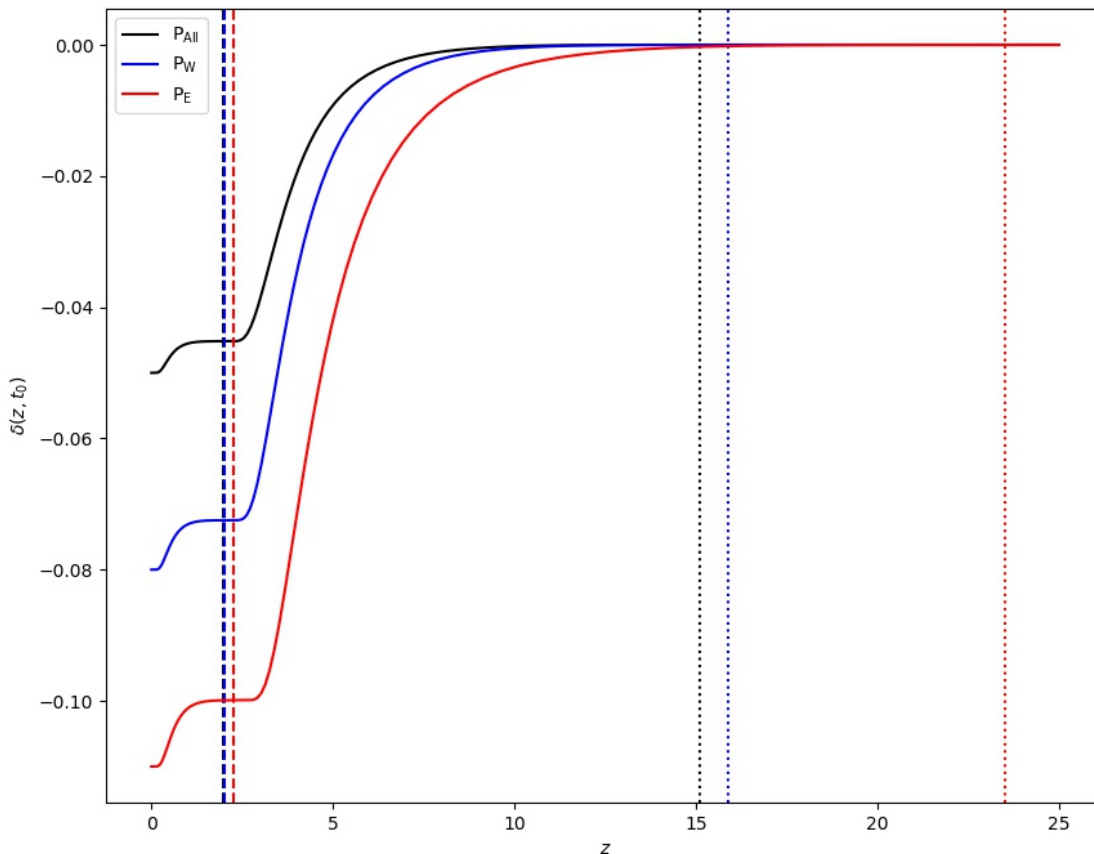


FIG. 7: The integrated mass density contrast $\delta(z, t_0)$ for no cut case and one vertical cut case, where $\delta_0 = -0.05$ (black solid), $z_C = 1.97$ (black dashed) and $z_B = 15.1$ (black dotted) for P_{All} , $\delta_0 = -0.08$ (blue solid), $z_C = 2.02$ (blue dashed) and $z_B = 15.9$ (blue dotted) for P_{W} and $\delta_0 = -0.11$ (red solid), $z_C = 2.28$ (red dashed) and $z_B = 23.5$ (red dotted) for P_{E} respectively.

- [20] A. Mariano and L. Perivolaropoulos, “Is there correlation between Fine Structure and Dark Energy Cosmic Dipoles?,” *Phys. Rev. D* **86**, 083517 (2012) [arXiv:1206.4055 [astro-ph.CO]].
- [21] H. N. Lin, S. Wang, Z. Chang and X. Li, “Testing the isotropy of the Universe by using the JLA compilation of type-Ia supernovae,” *Mon. Not. Roy. Astron. Soc.* **456**, no.2, 1881-1885 (2016) [arXiv:1504.03428 [astro-ph.CO]].
- [22] D. Zhao, Y. Zhou and Z. Chang, “Anisotropy of the Universe via the Pantheon supernovae sample revisited,” *Mon. Not. Roy. Astron. Soc.* **486**, no.4, 5679-5689 (2019) [arXiv:1903.12401 [astro-ph.CO]].
- [23] J. Garcia-Bellido and T. Haugboelle, “Confronting Lemaitre-Tolman-Bondi models with Observational Cosmology,” *JCAP* **04**, 003 (2008) [arXiv:0802.1523 [astro-ph]].
- [24] W. Valkenburg, V. Marra and C. Clarkson, “Testing the Copernican principle by constraining spatial homogeneity,” *Mon. Not. Roy. Astron. Soc.* **438**, L6-L10 (2014) [arXiv:1209.4078 [astro-ph.CO]].
- [25] B. Audren, J. Lesgourgues, K. Benabed and S. Prunet, “Conservative Constraints on Early Cosmology: an illustration of the Monte Python cosmological parameter inference code,” *JCAP* **02**, 001 (2013) [arXiv:1210.7183 [astro-ph.CO]].
- [26] W. Valkenburg, “Complete solutions to the metric of spherically collapsing dust in an expanding spacetime with a cosmological constant,” *Gen. Rel. Grav.* **44**, 2449-2476 (2012) [arXiv:1104.1082 [gr-qc]].
- [27] D. Blas, J. Lesgourgues and T. Tram, “The Cosmic Linear Anisotropy Solving System (CLASS) II: Approximation schemes,” *JCAP* **07**, 034 (2011) [arXiv:1104.2933 [astro-ph.CO]].
- [28] A. Lewis, “GetDist: a Python package for analysing Monte Carlo samples,” [arXiv:1910.13970 [astro-ph.IM]].

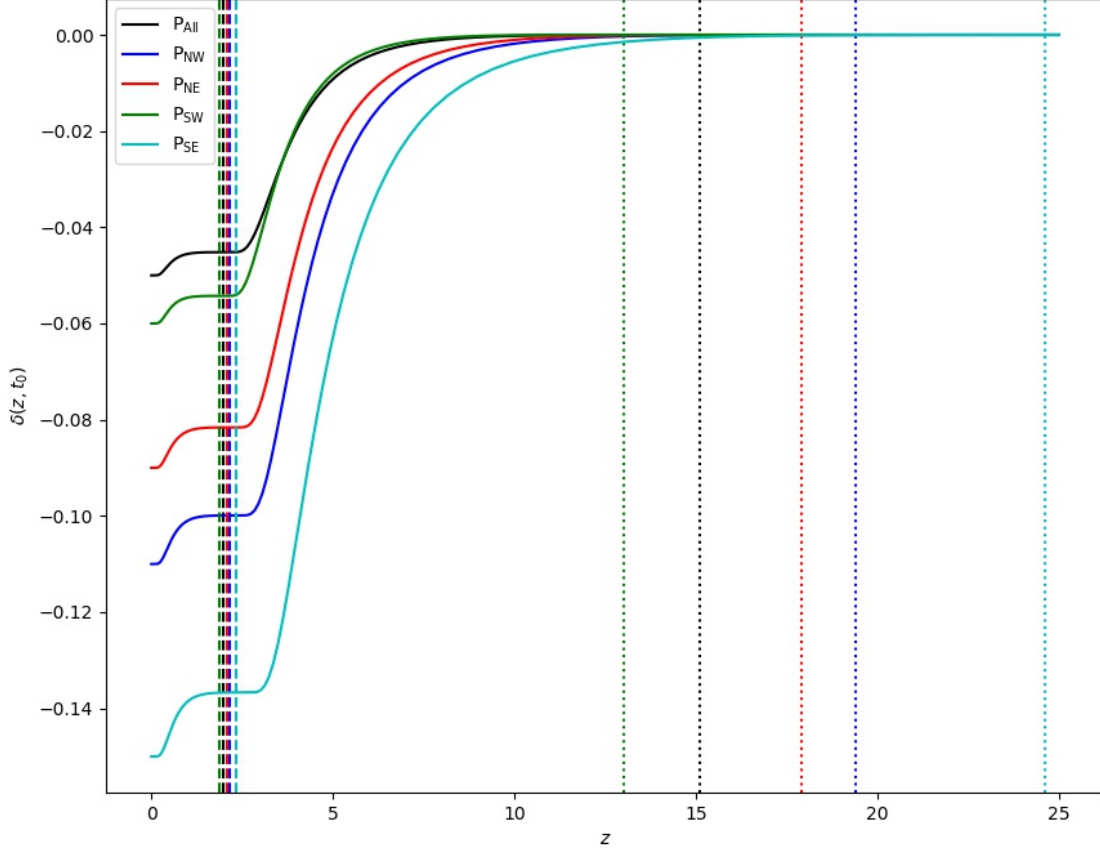


FIG. 8: The integrated mass density contrast $\delta(z, t_0)$ for no cut case and two cuts case, where $\delta_0 = -0.05$ (black solid), $z_C = 1.97$ (black dashed) and $z_B = 15.1$ (black dotted) for P_{All} , $\delta_0 = -0.11$ (blue solid), $z_C = 2.16$ (blue dashed) and $z_B = 19.4$ (blue dotted) for P_{NW} , $\delta_0 = -0.09$ (red solid), $z_C = 2.10$ (red dashed) and $z_B = 17.9$ (red dotted) for P_{NE} , $\delta_0 = -0.06$ (green solid), $z_C = 1.88$ (green dashed) and $z_B = 13.0$ (green dotted) for P_{SW} and $\delta_0 = -0.15$ (cyan solid), $z_C = 2.34$ (cyan dashed) and $z_B = 24.6$ (cyan dotted) for P_{SE} respectively.